Spatially and temporally non-uniform plasmas : microdischarges from the perspective of molecules in a packed bed plasma reactor

Spatially and temporally non-uniform plasmas: microdischarges from the perspective of molecules in a packed bed plasma reactor

K. van 't Veer[1,2,*], S. van Alphen[1,3], A. Remy[2,4], Y. Gorbanev[1], N. De Geyter[4], R. Snyders[3,5], F. Reniers[2], A. Bogaerts[1,*]

[1]*University of Antwerp, Department of Chemistry, Research Group PLASMANT, Universiteitsplein 1, 2610 Wilrijk-Antwerp, Belgium*

[2]*Université Libre de Bruxelles, Faculty of Sciences, Chemistry of Surfaces, Interfaces and Nanomaterials, CP255, Avenue F. D. Roosevelt 50, B-1050 Brussels, Belgium*

[3]*Université de Mons, Plasma Surface Interaction Chemistry, Place du Parc 23, 7000 Mons, Belgium*

[4]*Ghent University, Faculty of Engineering and Architecture, Department of Applied Physics, Research Unit Plasma Technology (RUPT), Sint-Pietersnieuwstraat 41 B4, 9000 Ghent, Belgium*

[5]*Materia Nova Research Center, 1 Avenue Nicolas Copernic, B 7000 Mons, Belgium*

[*]E-mail: kevin.vantveer@uantwerpen.be, annemie.bogaerts@uantwerpen.be

Abstract

Dielectric barrier discharges (DBDs) typically operate in the filamentary regime and thus exhibit great spatial and temporal non-uniformity. In order to optimize DBDs for various applications, such as in plasma catalysis, more fundamental insight is needed. Here, we consider how the millions of microdischarges, characteristic for a DBD, influence individual gas molecules. We use a Monte Carlo approach to determine the number of microdischarges to which a single molecule would be exposed, by means of particle tracing simulations through a full-scale packed bed DBD reactor, as well as an empty DBD reactor. We find that the fraction of microdischarges to which the molecules are exposed can be approximated as the microdischarge volume over the entire reactor gas volume. The use of this concept provides good agreement between a plasma-catalytic kinetics model and experiments for plasma-catalytic NH_3 synthesis. We also show that the concept of the fraction of microdischarges indicates the efficiency by which the plasma power is transferred to the gas molecules. This generalised concept is also applicable for other spatially and temporally non-uniform plasmas.

1. Introduction

Plasma catalysis is gaining a lot of interest for many applications, but the underlying mechanisms are far from being understood [1]. The most common plasma source in plasma catalysis is a dielectric barrier discharge (DBD) [2], which typically operates in the filamentary regime. This means that the plasma exhibits a great spatial and temporal non-uniformity, in the form of millions of microdischarges taking place throughout the whole reactor [3]. A better understanding of how these millions of microdischarges interact with the individual molecules in the plasma is very important, considering the complex reaction kinetics associated with typical gas conversion processes [4]–[6]. These complex

chemistries are typically modelled by so-called 0D or global plasma models, in which no explicit spatial dependency of the plasma is taken into account [7].

In order to capture the characteristics of a filamentary DBD in 0D plasma kinetics models, various authors have adopted a certain microdischarge frequency [8]–[12], and later specifically applied a so-called volume-corrected microdischarge frequency [13], [14]. The latter takes into account that a molecule does not experience all the microdischarges due to the stochastic behaviour of these microdischarges [15]. This quantity was defined as the microdischarge volume over the reactor volume [13], [14].

In this paper we substantiate this idea, as the fraction of microdischarges to which individual molecules are exposed, and we employ a Monte Carlo approach to calculate this fraction of microdischarges. The Monte Carlo calculations consider particle trajectories through a reactor volume, based on a full-scale flow model of a packed bed and empty DBD reactor, which will be discussed in detail. Furthermore, we report ICCD images to substantiate the assumptions underlying our calculations and we use a plasma kinetic model and plasma catalysis experiments to validate our concept of the fraction of microdischarges. Finally, we discuss the general applicability of our findings. The fraction of microdischarges can be related to the efficiency by which the plasma power is transferred to the individual gas molecules in the plasma reactor.

2. Methods

2.1. Particle tracing

To obtain realistic trajectories of gas molecules flowing through a typical plasma reactor, as input to our Monte Carlo calculations (section 2.2), we performed computational fluid dynamics (CFD) followed by particle tracing simulations.

The CFD model describes the behaviour of a pure N_2 gas flow in both an empty and a packed bed cylindrical DBD reactor. Modelling pure N_2, as opposed to a specific N_2-H_2 mixture, will deliver a general overview for N_2-containing gas flows, while avoiding the need for approximative theories for calculating gas mixture properties like the viscosity [16]. The CFD model solves the mass continuity and momentum continuity Navier-Stokes equations for an incompressible Newtonian fluid:

$$\rho \nabla . \overrightarrow{u_g} = 0 \tag{1}$$

$$\rho\left(\overrightarrow{u_g} \cdot \nabla\right)\overrightarrow{u_g} = \nabla \cdot \left[-p\vec{I} + (\mu + \mu_T)\left(\nabla\overrightarrow{u_g} + \nabla\left(\overrightarrow{u_g}\right)^T\right)\right] + \vec{F} \tag{2}$$

where ρ stands for the gas density, $\overrightarrow{u_g}$ is the gas flow velocity vector, superscript T stands for transposition, p is the gas pressure, μ is the dynamic viscosity and μ_T the turbulent viscosity of the fluid, $\vec{I}$ is the unity tensor and $\vec{F}$ is the body force vector.

In an empty reactor, the flow is expected to be highly laminar, which greatly reduces the complexity of equations 1 and 2, as we can consider $\mu_T = 0$.

To be prepared for any turbulence occurring when a packing is added to the reactor geometry, the turbulent properties of the flow were solved for in the packed bed DBD reactor. We achieved this by using a Reynolds-averaged-Navier-Stokes (RANS) turbulent model, which significantly reduces the computation time by averaging all fluctuating turbulent quantities (i.e., the turbulent kinetic energy and the turbulent dissipation rate) over time. We used the k-ω model, as this model is still applicable at low level of turbulence and is able to resolve the laminar boundary layer near the walls [17]. This is important for the flow inside a packed bed reactor, as contact with the beads will introduce a lot of these boundary layers.

To reduce the large computational time of the CFD calculations, especially regarding the complexity due to the introduction of 13,216 beads inside the geometry, several measures were taken to reduce the number of finite mesh elements in the modelled geometry. First, the axial symmetry allows us to consider only 1/8th of the reactor, reducing the complexity of the model to 1,652 beads. Secondly, to avoid the need for a very small finite element mesh to resolve the contact points between two beads, the radius of the beads was reduced by 5 % for the flow calculation.

After the CFD calculations, we performed particle tracing simulations, in which we computed the trajectory of gas molecules as they flow through the reactor. These trajectories are calculated based on Newton's law of motion, using the drag force imposed by the velocity fields that were previously computed:

$$\frac{d\left(m_p \overrightarrow{u_g}\right)}{dt} = \overrightarrow{F_D} \tag{3}$$

where m_p is the particle's mass, $\overrightarrow{u_g}$ is the gas flow velocity vector and $\overrightarrow{F_D}$ the drag force.

We performed the trajectory calculations for 10,000 particles, i.e., gas molecules, to ensure statistically relevant results. This yields 10,000 possible trajectories which the gas molecules can follow when flowing through either the empty or the packed bed DBD reactor. However, the solver removes trajectories from the simulation when the particles get stuck on a wall, due to their velocity which can approximate 0 m/s upon collisions with the walls. This is especially quite significant in a packed bed DBD where the particles often collide with the beads, but more than 5,000 particle trajectories were still preserved in the simulation. Those remaining trajectories do also include collisions. The calculated trajectories served as input to our Monte Carlo calculations (section 2.2) from which we determined the fraction of microdischarges experienced by the gas molecules.

Both the CFD and the particle tracing calculations were solved using the CFD module of COMSOL version 5.5 [18]. We used the same residence time in the empty and packed bed reactor (see section 3.1.1).

The flow simulations do not account for plasma effects, because we consider a full scale packed bed reactor with approximately 13,000 beads in the reactor (see above), and the complexity of a plasma model on this scale would be too high.

2.2. Monte Carlo calculations

The Monte Carlo approach determines whether a particle along a specific trajectory through the reactor (see section 2.1) is hit by a microdischarge, which occurs randomly throughout the reactor.

The total number of microdischarge events that take place in a DBD reactor is typically in the order of a few millions. Because the microdischarges occur throughout the whole reactor and because single gas molecules can only be at one point in the reactor at any moment in time, we expect that they experience a reduced number of microdischarges. For this reason we employed a Monte Carlo approach to statistically determine the fraction of microdischarges to which the individual gas molecules are exposed. Hence, by the general Monte Carlo approach, we select random numbers between 0 and 1, which determine at which location a microdischarge occurs. We assume that the locations of the microdischarge events are uniformly distributed throughout the reactor gas volume (see next section for motivation), but their actual occurrence is determined randomly. We performed experimental diagnostics to show that a uniform distribution of the microdischarges throughout the reactor is indeed a good approximation (see section 2.3 and 3.3). For more details on the placement of the microdischarge events, we refer to section 3.2.

Furthermore, the microdischarge events are equally distributed over the gas residence time and the microdischarges stay active for a certain microdischarge lifetime. For each trajectory through the reactor we check whether or not a particle (i.e., gas molecule) is at the same location as a microdischarge at any moment in time during which the specific microdischarge is active. If this is the case, we define a hit for the microdischarge event. The total number of hits per trajectory over the total number of microdischarges that took place in the reactor will then define the fraction of microdischarges.

We acknowledge that we do not capture the actual physics of a microdischarge, and we do not consider an actual plasma, which could influence charged particles, especially in the microdischarges due to the presence of strong electric fields. Indeed, self-consistent modelling of a filamentary plasma is a difficult task, requiring e.g., particle-in-cell Monte Carlo methods [19]. As we consider millions of random microdischarges instead of individual microdischarges, a fully self-consistent filamentary plasma model is not feasible. However, we do apply this concept of the fraction of microdischarges in a 0D plasma kinetics model (section 2.4).

Finally, we note that our Monte Carlo calculation and the present study lead to general insights that are not necessary specific to a single experimental setup. As long as the assumption on the uniform distribution of the microdischarges is valid, the findings will be unaltered and our Monte Carlo calculations should not have to be repeated. The conclusions are used in our 0D plasma kinetics model. Thus overall, the modelling scheme and the modelling presented in this paper is quite different from particle-in-cell Monte Carlo calculations. Indeed, the latter self-consistently describe the microscopic behavior of individual particles, i.e., their collisions and movement in an electric field, which is influenced by the space charge generated by the super-particles, hence completely different from our model. Moreover, they typically focus on the detailed discharge behaviour of a single, or a few, filaments, and not on the overall gas conversion process (like in our plasma kinetic modelling).

2.3. Experiments

In the Monte Carlo calculations we assume that the microdischarges are uniformly distributed throughout the plasma reactor. We verified this assumption by means of experimental diagnostics.

The reactor used to study the distribution of microdischarges by ICCD images is a closed parallel plate rectangular DBD reactor with two dielectrics. Each dielectric is a fused silica (quartz) piece of 118 x 68 x 3 mm^3. A discharge gap of 2 mm is formed between them. On each outer side, the dielectrics are covered by a stainless-steel mesh acting as electrode. The structural parts of the reactor, i.e., the enclosure, are built in transparent polymethyl methacrylate (PMMA). This configuration allows to place a high-speed camera perpendicular to the dielectric surface and to have a clear view of the discharge (as illustrated in figure 1).

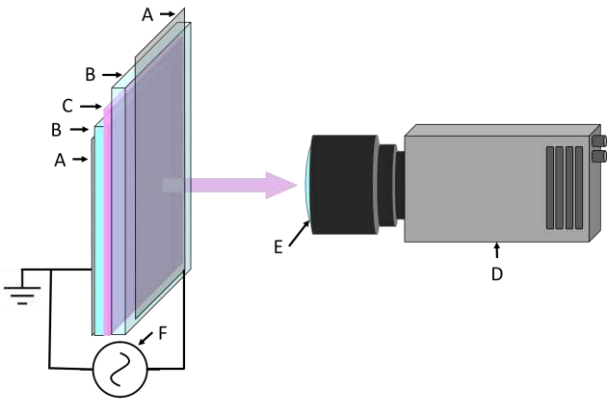

Figure 1. Schematic of the DBD setup used for ICCD imaging, showing the electrodes (A), dielectric barriers (B), discharge gap (C), camera body (D), lens (E) and high voltage generator (F).

One of the electrodes is connected to a high voltage generator (AFS G10S-V) through a high frequency transformer (1-30 kHz), while the other electrode is grounded. The generator allows to control the operating frequency and the applied power in the plasma. The experiments were conducted at a frequency of 12 kHz and a power of 100 W. Approximately 60% of this power is effectively absorbed into the plasma. A constant flow rate of 1 L/min of a N_2:O_2 gas mixture with a ratio of 1:1 (500 mL/min

each) is applied at atmospheric pressure. The high-speed camera used for ICCD imaging is a Photron Nova S2 working at 10,000 frames per second (fps) at a raw resolution of 1024 x 672 pixels. The final resolution is divided by two after application of a binning 2 x 2 to enhance the luminosity of the plasma, giving a final resolution of 512 x 336 pixels.

Furthermore, we studied the effect of the fraction of microdischarges in a plasma kinetics model (see section 2.4). We performed plasma-catalytic ammonia synthesis experiments to verify whether our plasma kinetics model is realistic. The ammonia synthesis experiments were performed in an axial cylindrical DBD reactor operated at atmospheric pressure, 23.5 kHz frequency and ca. 10 kV peak-to-peak voltage, and a gas mixture of H_2:N_2 with a ratio of 1:1. The applied voltage correspond to 100 W of supplied power of which approximately 70 % goes into the plasma. The catalyst was 10 wt% Co/Al_2O_3 prepared via incipient wetness impregnation of commercial Al_2O_3 beads (diameter: 1.8 mm, Sasol). The production of NH_3 was monitored by mass spectrometry of the outlet gaseous mixture. The full description of the reactor, plasma discharge, experimental procedure, analytical techniques, and catalyst preparation and characterisation is found elsewhere [20].

In our experiments, the total gas flow rate was varied from 100 to 400 mL/min to allow different values of the gas residence time inside the plasma region (see section 3.4).

2.4. Plasma kinetics model

We use our previous 0D plasma chemistry model [21] developed within ZDPlasKin [22] and catalytic surface chemistry microkinetics model [21] to investigate the effect of using different fractions of microdischarges and we compare the results against experiments (see section 2.3). In this model we solved the continuity equation for the various plasma and surface species:

$$\frac{dn_i}{dt} = \sum_r c_{i,r} \left(k_r \prod_l n_l \right) \tag{8}$$

where n_i is the density of species i, c is the stochiometric number of the species in reaction r, k_r is the rate coefficient and the subscript l represents the species on the left hand side of the reaction. The rate coefficients of the catalytic surface reactions are adopted from Engelmann et al. [20]. The gas phase rate coefficients are adopted from literature and reported in [21]; they are constant or depend on the gas temperature or electron temperature. The rate coefficients of electron impact reactions are evaluated from electron impact cross sections using BOLSIG+ [23], which solves the Boltzmann equation for the electrons to obtain the electron energy distribution function $f(\mathbf{r}, \mathbf{v}, t)$ (EEDF):

$$\frac{\partial f}{\partial t} + \mathbf{v} \cdot \nabla f - \frac{e}{m} \mathbf{E} \cdot \nabla_{\mathbf{v}} f = C \tag{9}$$

where e is the elementary charge, m is the electron mass, $\mathbf{v}$ is the velocity vector, $\nabla_{\mathbf{v}}$ is the velocity-gradient and C contains the actual electron impact collision terms; for more details, we refer to Hagelaar and Pitchford [23]. The EEDF is calculated based on the collisions and electric field. The collisions are defined by the cross sections, and in our model we provide the reduced electric field E/N based on the power density P/V of the plasma [15], [21]:

$$E/N = \frac{1}{N}\sqrt{\frac{P/V}{en_e\mu_e}} \tag{10}$$

where N is the total gas number density and μ_e is the electron mobility calculated from the EEDF [23]. Because of the calculation of the mobility, first an initial set value for the reduced electric field is used.

In order to capture the properties of a filamentary DBD, we describe the microdischarges as triangular power density pulses with a certain lifetime, adopted from the experimental instantaneous plasma power and an assumed microdischarge volume [21]. Such pulses indeed provide reduced electric fields, electron densities and electron temperatures as expected for filamentary DBDs [8], [10]. We note that in our model there is also an active plasma in between the microdischarges, but much weaker than the actual microdischarges themselves. From the same data we determine the number of microdischarges per half cycle ($N_{MD,½\,cycle}$) [21]. Within the gas residence time in the reactor, we can then approximate the total number of microdischarges in the reactor with:

$$N_{MD,total} = 2N_{MD,½\,cycle}f_D\tau_{res} \tag{4}$$

where N_{MD} is the number of microdischarges in the whole reactor, during the full residence time (subscript $total$) and during one discharge half cycle (subscript ½ $cycle$), f_D is the discharge frequency and τ_{res} is the residence time. This typically yields in the order of millions of microdischarges (i.e., by using typical values of $N_{MD,½\,cycle}$ = 25, f_D = 23.5 kHz and τ_{res} = 4 s [21]).

In plasma kinetics models of a DBD only a small fraction of those microdischarges are assumed to be experienced by the molecules [8]–[15]. The reduced number of microdischarges that are actually considered in the model can be described with:

$$N_{MD,reduced} = \eta_{MD}N_{MD,total} \tag{5}$$

where we introduce η_{MD}, the fraction of microdischarges to which individual gas molecules are exposed, which we determine in this study using the Monte Carlo approach (see section 2.2).

In our previous work we assumed that the fraction of microdischarges depends on the gas velocity and the amount of reactor volume passed through by the gas molecules during one discharge period. This caused the number of microdischarges in the model to be independent of the residence time [15]. In

earlier work by our group PLASMANT, it was assumed that the fraction of microdischarges is given by the microdischarge volume over the reactor volume [13], [14].

We will use this plasma kinetics model to investigate the effect of varying the fraction of microdischarges over a large range (section 3.4).

3. Results and discussion

3.1. Particle tracing

3.1.1. Particle trajectories through an axial cylindrical packed bed reactor

We calculated particle trajectories through both an empty and packed bed cylindrically symmetrical DBD reactor, as described in section 2.1. The flow rate in the empty DBD was adjusted relative to the one in the packed bed DBD, to account for the reduced volume due to the packing in the latter, and to obtain the same average residence time in both reactors. The empty reactor volume is approximately 9.42 cm^3 and the packing volume is approximately 5.93 cm^3 (i.e., 13,216 spheres with 1 mm diameter), yielding a packing factor of 63 %. This results in a flow rate of 270 ml/min for the empty reactor, based on a 100 ml/min flow rate in the packed bed reactor. Using those different flow rates, the average residence time in both reactors is then 2.1 s. In figure 2 we show the packed bed reactor, the dimensions of the packing, as well as the simulated gas molecules and their velocity. The figure shows that gas molecules flow through the reactor at a wide range of velocities, varying from 0.002 m/s to 0.1 m/s.

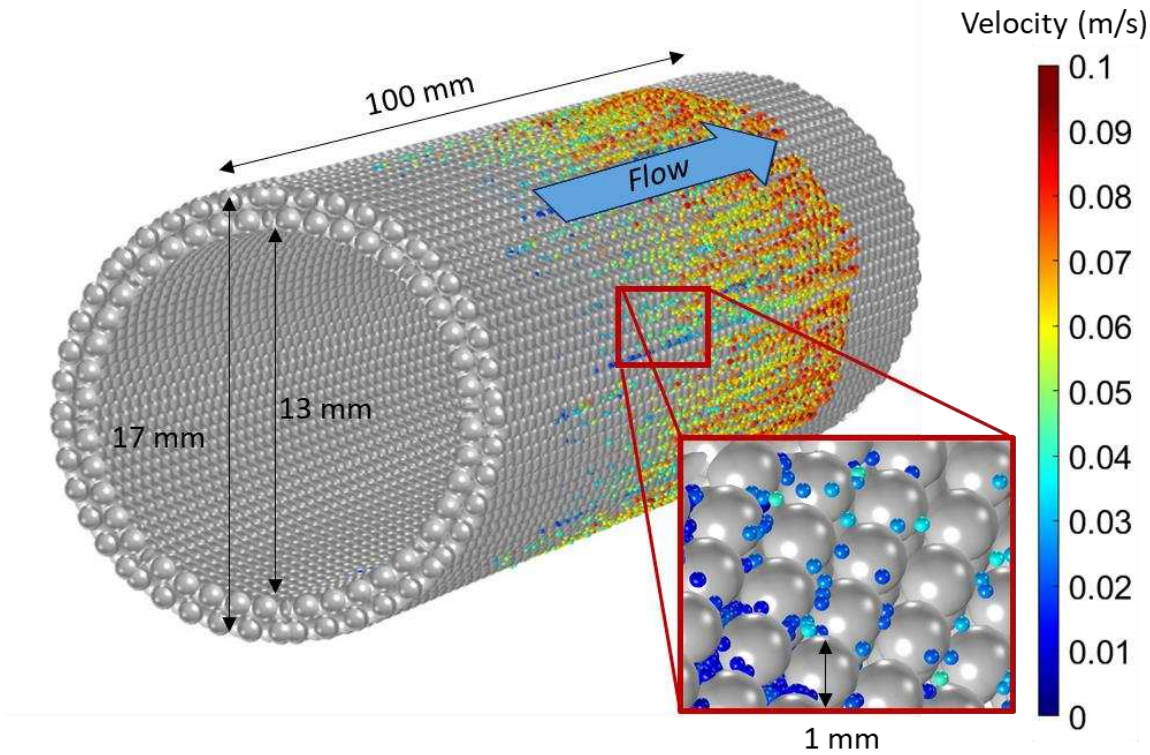

Figure 2. Illustration of the gas molecules flowing through a packed bed reactor consisting of two concentric cylinders. The reactor contains 13,216 spherical beads (1 mm in diameter) stacked into two layers in the gap between both concentric cylinders. Note that the reactor diameter and reactor length are not to scale, for clarity. The inner diameter of the large cylinder is 17 mm, while the outer diameter of the small cylinder is 13 mm, yielding a gaseous gap of 2 mm.

3.1.2. Residence time distribution in an empty and packed bed DBD reactor

In figure 3a and 3b, we show the residence time distribution of the gas based on the particle tracing calculations for an empty and a packed bed DBD reactor, respectively. Besides the tail of the distribution, which is less smooth in case of the packed reactor, the distributions are quite similar. Indeed, the flow rate was chosen to yield the same average residence time in both reactors (see section 3.1.1).

The gas flow in an empty reactor follows a typical Poiseuille velocity profile, as illustrated in figure 4a. As a result of the fluid viscosity, friction between the flowing gas and the reactor wall causes the gas to slow down close to the wall, creating a boundary layer that shapes the parabolic velocity profile. Hence, the molecules in vicinity to the reactor walls in the empty reactor are characterized by a longer residence time compared to the average. The molecules in the middle of the reactor have a high velocity and account for the shorter residence times, resulting in the distribution as shown in figure 3a.

The gas flow in the packed reactor shows opposite behaviour, as illustrated in figure 4b. Fast molecules, with short residence times, now flow through the reactor in the vicinity of the wall, while the slow molecules, with long residence times, flow through the middle of the reactor. This effect is discussed in greater detail below (section 3.1.3).

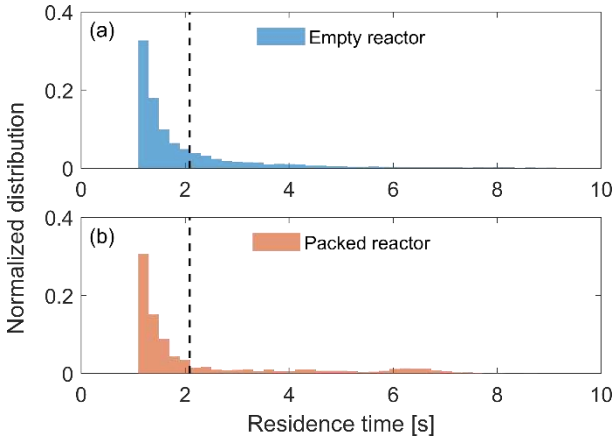

Figure 3. Residence time distribution in the empty (a) and packed bed (b) reactor. The average residence time is the same in both reactors, and is indicated with a vertical dashed line (approximately 2.1 s).

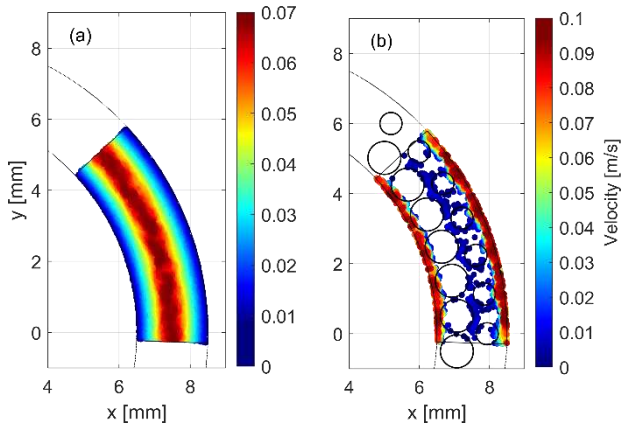

Figure 4. Top view of the axial velocity of each particle in the empty (a) and packed bed (b) reactor. The white space outside of the packing bead contours in (b) represents locations where the probability of finding a particle is so low that none of the simulated particles were found there. Note, both figures show a cross section of the reactor made at a specific axial height (z = 90 mm, i.e., 10 mm before the reactor outlet). In (b) the intersection of this plane with the packing beads does not cut the beads equally because the two layers are not aligned in a closed packing of equal spheres, hence the outer layer of beads exhibits a smaller radius.

3.1.3. Gas distribution in an empty and packed bed DBD reactor

When a packed bed is introduced in the reactor, the incoming gas is forced to flow through the small gaps in between the beads of the packed bed, which drastically changes the distribution of the gas flow compared to an empty reactor. In figure 5 we present the gas distribution for an empty and a packed bed DBD reactor, as calculated by the particle tracing simulations. For an empty reactor, figure 5a shows that most of the gas passes through the centre of the reactor, where the flow is undisturbed by the viscous boundary layer near the walls. As shown by figure 5b, the introduction of a packed bed seemingly inverts this profile, as the flow is redistributed towards the reactor walls. The gas flow favours the path of least resistance and thus avoids the darkest blue zones around r = 7.1 mm and r = 7.9 mm, where the two bead layers are located (cf. figure 4b). The small gaps between the beads only allow for small flow rates through the bed, so approximately 90% of the gas molecules flows towards the outer layer of the bed and the reactor wall, where the gaps are larger than in the perfectly packed centre. This value is based on integrating the probability distribution at the end of the reactor (figure 5b at z = 100 mm) and comparing the outer layers to the middle section (between a radius of 6.9 and 7.9 mm), where the average probability of finding a gas molecule is 0.006 compared to 0.1 in the outer layers.

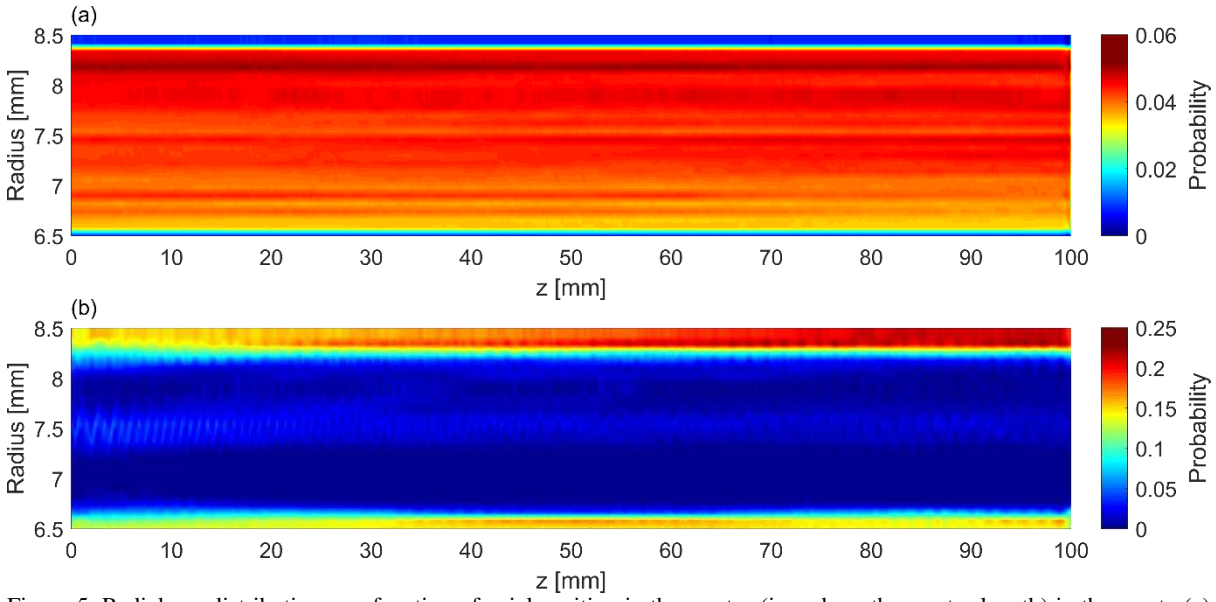

Figure 5. Radial gas distribution as a function of axial position in the reactor (i.e., along the reactor length) in the empty (a) and packed bed (b) reactor. The radial distribution was normalized at each axial position in the reactor, so integration along a vertical line in the figure equals to 1.

Figure 5a and 5b both show that the gas density near the outer wall (towards 8.5 mm radius) is slightly higher than the gas density near the inner wall (6.5 mm radius). This is due to the curve of the cylindrical DBD reactor. Indeed, there can be more gas molecules at the larger radius due to the larger volume (or circumference). For the packed bed reactor this effect is larger, as also the packing configuration has to be considered. This is illustrated in figure 6, which shows the close packing of equal spheres for a packed bed DBD reactor both with a straight and a curved electrode. The figure demonstrates that a curved electrode introduces more space (highlighted in red) between the beads in the upper bead layer, allowing for more gas to flow through.

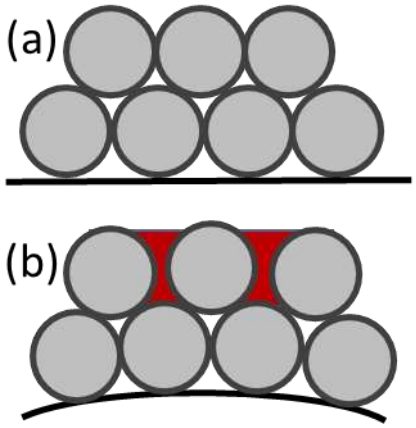

Figure 6. Close packing of equal spheres for a packed bed DBD reactor with a straight (a) and a curved (b) electrode surface.

The fact that the incoming gas is not evenly distributed over the reactor bed could be an important consideration for catalytic processes in packed bed DBD plasma reactors. Only a smaller portion of the gas will flow through the middle of the bed, i.e., in between the two bead layers, where there is more

contact with the catalyst bed, and a longer residence time in the plasma (see previous section). However, in reality, the ideal packing assumed in this model is unlikely due to the bead shape and size and the filling of the reactor. Thus, in reality, gaps of various sizes can be formed throughout the packed bed, which can also allow more gas to flow through the centre of the bed.

3.2. Monte Carlo calculations

3.2.1. Microdischarge distribution and "hits" in the empty and packed bed reactor

We calculated the fraction of microdischarges with the Monte Carlo approach explained in section 2.2, which we applied to the particle trajectories of the empty and packed bed DBD reactor (cf. section 3.1).

We assume 25 microdischarges per discharge half cycle, with a lifetime of 200 ns and a discharge frequency of 23.5 kHz [21]. With the maximum residence time of 9.41 s (corresponding to the empty reactor, cf. figure 4a), this gives 10,739,500 microdischarges taking place throughout the whole reactor, during the entire gas residence time in the reactor. The maximum residence time in the packed reactor was 8.63 s, corresponding to 10,140,250 microdischarges.

In the empty reactor, we assumed the microdischarges to be small channels between the inner and outer electrode. For simplicity, the channels are actually very thin circle sector, which allows us to use the cylindrical coordinate system throughout the Monte Carlo calculations. The azimuthal width of the microdischarges is 0.1 rad and the axial width is 0.1 mm. The channel length is approximately 2 mm, corresponding to an approximate microdischarge volume of 0.15 mm^3. For clarity, the definition of the circle sector and the thin microdischarge channel is shown in figure 7. The microdischarge events are placed randomly (as defined by the Monte Carlo approach) throughout the full reactor gas volume.

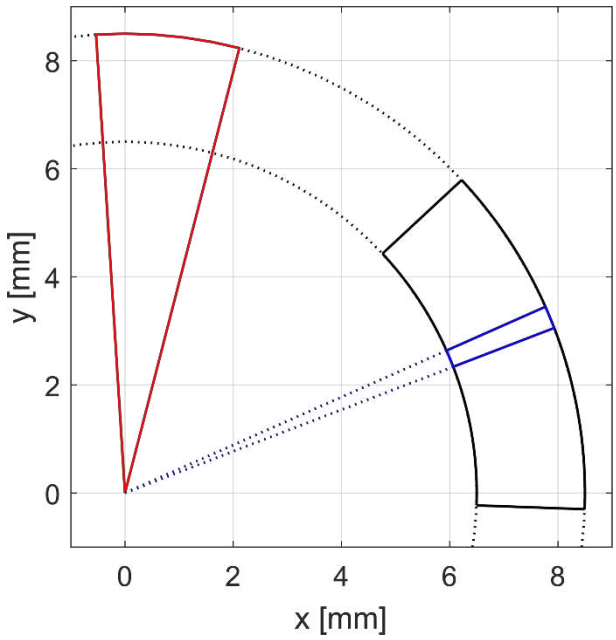

Figure 7. Schematic showing a top view of approximately 1/4th of the cylindrical reactor (dashed black lines), the geometrical definition of a circle sector (red outline), the modelled reactor segment (black outline) and a thin circle sector representing a microdischarge channel in the empty reactor (blue outline).

In the packed bed reactor, the microdischarge events are defined as spheres with 0.3 mm radius, corresponding to an approximate microdischarge volume of 0.11 mm^3 [21]. The events are uniformly distributed throughout the packed bed reactor by randomly choosing a packing bead and then randomly choosing a point on the surface of this specific bead. Filamentary DBDs, especially with packed beds, are often characterized by point-to-point discharges, i.e., microdischarges between two beads, or surface discharges, i.e., microdischarges over the surface of a packing bead [24]. Our chosen spherical microdischarge volumes, which we centre on the surface of the packing beads, can be considered a combination of both, as the chosen radius is also large enough to bridge the gaps between two close packing beads.

In figure 8, we illustrate the locations of all the microdischarge events throughout the reactors. Note that this figure only shows the locations and not the size (0.1 mm width and 0.3 mm radius in case of the empty and packed bed reactor, respectively) for the sake of clarity.

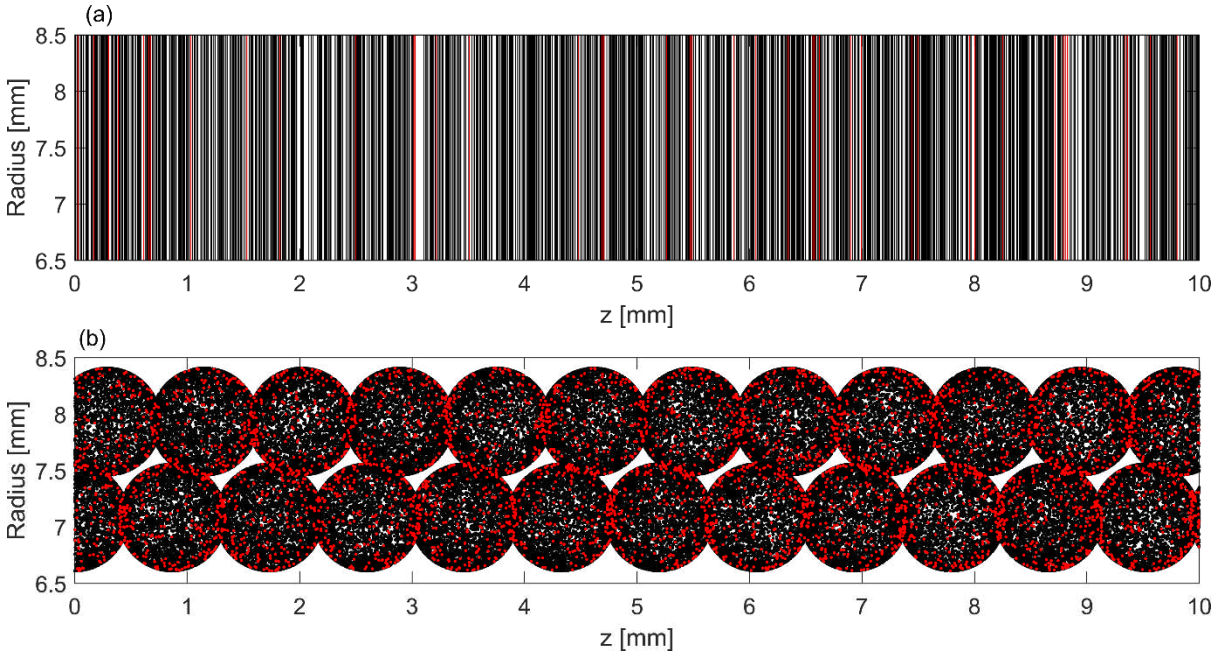

Figure 8. The microdischarge locations in both the empty (a) and the packed bed (b) DBD reactor. Only 1/10th of the reactor length is shown, with all of the microdischarges taking place (dark areas created by the overlapping and connecting individual vertical lines (a) or dots (b)). The red lines and dots indicate microdischarge events that have hit a particle trajectory. Note that in (a) only 1 % of all microdischarges are plotted for the sake of clarity. In addition, because in (b) the microdischarge events are placed on the surface of the packing beads, the shape of the packing beads is reflected back in this figure.

In figure 9, we show five randomly selected particle trajectories and only the microdischarges to which they were exposed in the empty and packed reactor. It is clear that a particle trajectory can experience a microdischarge event anywhere along its trajectory. In case of the packed bed reactor (figure 9b and 9c) particles (i.e., gas molecules) travelling near the walls are typically exposed to only a few microdischarges along their trajectory, while particles that travel through the centre of the packed bed reactor experience more microdischarges. This is due to the longer residence time, as discussed in

section 3.1, and because there are somewhat more microdischarge events in the middle of the reactor (at a radius of 7.5 mm), where the two packing bead layers are in contact with each other (cf. figure 8b, which showed all microdischarges that took place, also including microdischarge events that did not hit any of the thousands of traced particles).

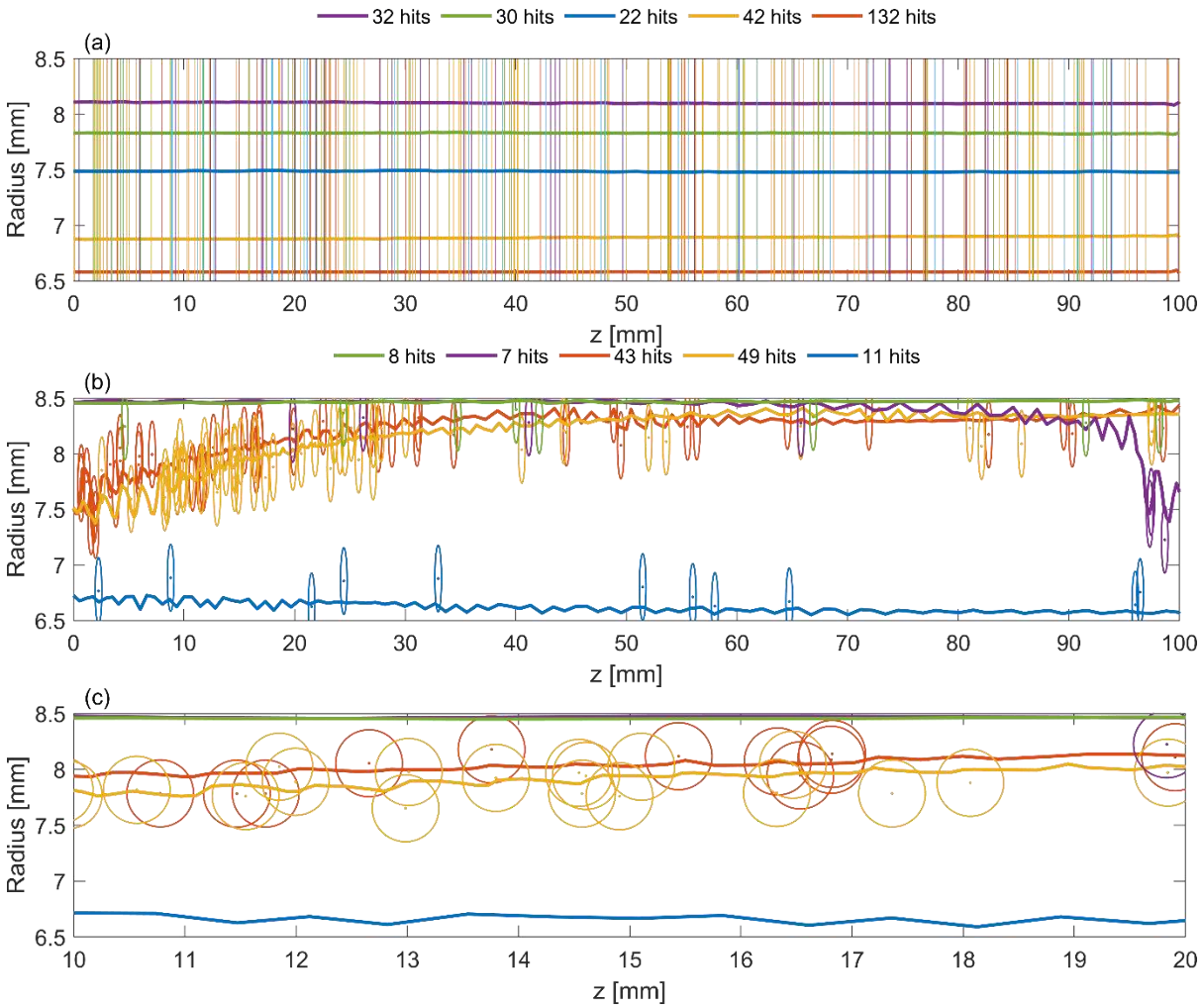

Figure 9. Five randomly selected particle trajectories flowing through the empty reactor (a) and the packed bed reactor (b, c), as well as the microdischarges to which they were exposed (vertical lines or spheres in the same colour). In (a) and (b) the full reactor length is shown (reactor length and radius not to scale). In (c) $1/10^{th}$ of the reactor length is shown (with reactor length and radius to scale), i.e., between z = 10 and 20 mm, where most of the hits occur for the orange and yellow trajectory, because those particle trajectories go here through the middle of the packed bed, where they move more slowly (cf. figure 4b), and there are slightly more microdischarge events.

In figure 10, we show that the hits between gas molecules and microdischarge events are also randomly distributed in time. We show this for the case of the packed bed, but it is also true for the empty reactor. Any gas molecule can have relatively short and long times between two microdischarges (cf. figure 10 for the same trajectories as in figure 9b). Note that the orange and yellow particle trajectories, which pass through the middle of the packed bed between z = 10 and 20 mm (cf. figure 9b) have a longer residence time (3.12 s and 3.03 s) and experience more microdischarges.

In section 3.1.2 and 3.1.3 we explained that most of the particles travel through the packed bed reactor in the outer layers (cf. figure 4b and 5b). Thus, only a few particles travel through the centre of the reactor, and experience a large number of microdischarges (cf. orange and yellow particle trajectories in figure 9b and 9c). Most particles will travel through the reactor near the electrode walls and experience only a few microdischarges.

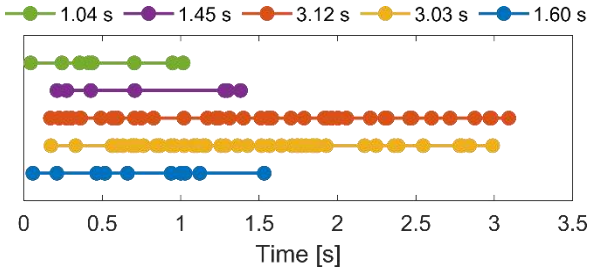

Figure 10. The moments in time at which the microdischarge event hits of figure 9b occurred (dots on the line) for each of the five particle trajectories. The legend indicates the residence time of each displayed trajectory.

The distribution of the time between two microdischarge hits, based on all trajectories and all successful microdischarge events, is given in figure 11. The median of this time distribution is 47 ms, the mode is 67 ms and the mean is 74 ms, the time between two microdischarge hits ranges from 68 µs to 1.1 s.

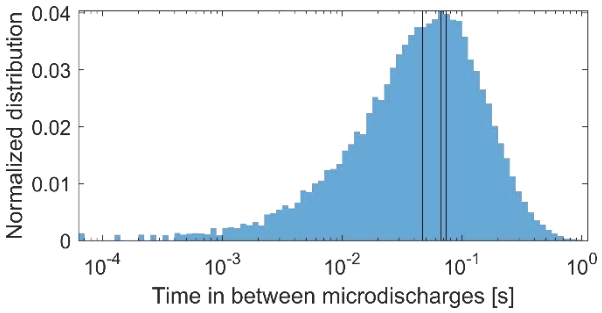

Figure 11. Distribution of the time between two microdischarge hits, when considering all trajectories. The vertical lines indicate, from left to right, the median (47 ms), mode (67 ms) and mean (74 ms), respectively.

3.2.2. Determination of the fraction of microdischarges to which the gas molecules are exposed

We use the results of each trajectory to determine the fraction of microdischarges to which the gas molecules are exposed, by fitting the Monte Carlo results of both the empty and packed bed reactor (see figure 12) to:

$$number\ of\ hits = x_1 \times \tau_{res} \tag{6}$$

where x_1 is the slope of the fit, from which the fraction of microdischarges can be evaluated based on equation 4 and 5 above:

$$\eta_{MD} = \frac{x_1}{2N_{MD,½\ cycle} f_D} \tag{7}$$

The fits are shown in figure 12. For each of the particle trajectories, we plot the number of microdischarge hits and their residence time. Each cross in figure 12 represents a particle trajectory. The slope of the fit through this plot of number of microdischarge hits vs the residence time gives us the value x_1 from equation 6 and from this slope we determine the fraction of microdischarges (equation 7).

Based on the slopes in figure 12 (i.e., the values of x_1) and equation 7, we calculate the fraction of microdischarges to which the gas molecules are exposed, as $(1.548 \pm 0.003)\times10^{-5}$ and $(1.306 \pm 0.006)\times10^{-5}$, for the empty and packed bed reactor, respectively.

Note that the linear fits go through the origin of the graphs, based on the expected relationship (cf. equation 6), but at longer residence times the fit does not seem optimal when enforcing this intersection at (0,0) for the packed bed reactor (figure 12b). Indeed, the points at longer residence time tend to lie above the fitted line. This is attributed to the fact that the slower particles move through the middle of the packed bed (cf. section 3.1), where there are slightly more microdischarge events, because the two packing bead layers are in contact with each other, hence explaining the slightly higher number of hits compared to the fitted line.

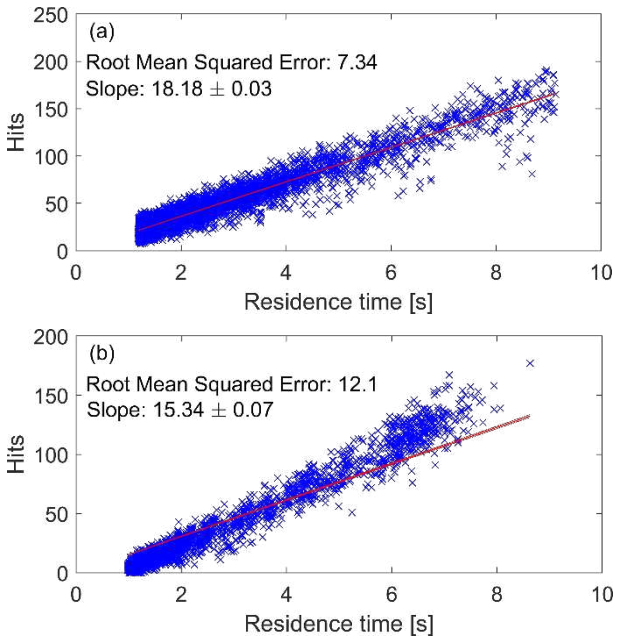

Figure 12. Number of microdischarge hits as a function of average residence time, for each of the particle trajectories, for the empty reactor (a) and the packed bed reactor (b). Each point corresponds to one trajectory. The data is fitted to equation 6, and the slope of the fit (x_1) is also indicated.

3.2.3. Empirical relationship for the fraction of microdischarges

As mentioned before, in earlier work from our group we assumed that the fraction of microdischarges to which the gas molecules are exposed, η_{MD}, is given by the microdischarge volume over the reactor volume [13], [14]. Based on the reactor volume $V_{reactor}$, the packing factor α and the microdischarge volume V_{MD} used in the COMSOL model and Monte Carlo calculations, we can also try to evaluate the fraction of microdischarges based on such volume-based relations:

$$\eta_{MD,empty} = \frac{V_{MD}}{V_{reactor}} \tag{11}$$

$$\eta_{MD,packed} = \frac{V_{MD}}{(1-\alpha)V_{reactor}} \tag{12}$$

With the microdischarge volume of 0.15 mm^3 and 0.11 mm^3 for the empty and packed bed reactor, respectively, the reactor volume of 9.42 cm^3 and the packing factor of 63 %, equation 11 and 12 calculate the fraction of microdischarges as 1.6×10^{-5} and 3.2×10^{-5} for the empty and packed bed reactor, respectively.

Hence, using this method, the fraction of microdischarges for the empty reactor is in very good agreement with the Monte Carlo results (i.e., 1.6×10^{-5} vs. $(1.548 \pm 0.003)\times10^{-5}$. On the other hand, the volume-based fraction of microdischarges for the packed bed reactor is somewhat overestimated compared to the Monte Carlo calculation (i.e., 3.2×10^{-5} vs $(1.306 \pm 0.006)\times10^{-5}$). However, in this case we need to take into account that the effective microdischarge volume used in the Monte Carlo calculations is somewhat lower than 0.11 mm³, due to the placement of the spherical microdischarge events on the surface of the packing beads and because the assumed microdischarge radius is larger than the smallest distance between the packing beads. If we account for this in equation 12 (by assuming $V_{MD}/2$ instead of V_{MD}), we obtain a fraction of microdischarges of 1.6×10^{-5}, which shows a much better agreement with the Monte Carlo results. We note that the fraction ½ is just an approximation. Indeed, in our Monte Carlo calculations for the packed bed reactor, we did place the spherical microdischarge events with an actual size of 0.11 mm^3 and the exact effective microdischarge volume is difficult to determine due to the complexity of the geometry of the packing beads and the stochastic nature of the calculation. The empty reactor (discussed above) is a much simpler case, as only the reactor walls give rise to a smaller effective microdischarge size.

It is clear that, in the case of a packed bed reactor, a direct comparison between the proposed simple relationship (of microdischarge volume over reactor volume) and the Monte Carlo calculations applied to a realistic reactor set-up is difficult, due to the definition of the microdischarge events, both in terms of their size and where they take place. However, the fact that the simple relationship predicts values close to the more explicit derivation based on the particle trajectories and Monte Carlo calculations,

especially for the empty reactor, is quite striking. Hence, we believe that the fraction of microdischarges to which the gas molecules are exposed, can be properly approximated by the microdischarge volume over the reactor gas volume.

Such a relationship between the microdischarge volume, reactor gas volume and fraction of microdischarges experienced by the molecules can be understood by the following explanation. If the microdischarges can occur throughout the reactor with the same probability, we can consider that, on average, the microdischarges always take place in the same point of the reactor. This is true for any point in the reactor and thus also any point that will be crossed by a gas molecule.

Multiple microdischarges occurring at the same time would not increase the probability for gas molecules of being hit by a microdischarge. Indeed, when multiple microdischarges occur at the same time but at different places, it is clear that a molecule can only experience one of these microdischarges at most.

3.3. Experimentally observed microdischarge distributions

In the previous section, we calculated the fraction of microdischarges based on a Monte Carlo approach, assuming a uniform distribution of the microdischarges. Various authors have recorded DBD plasma in both empty reactors [3] and packed bed reactors [24]–[27]. Wang et al. specifically reported their DBD plasma to become more uniform upon introducing a packing [28].

We made ICCD recording of a filamentary DBD plasma in an empty reactor. A transparent top electrode and dielectric allowed to record the microdischarges from above, as depicted in figure 13. We show a standard photograph of the plasma (a), as well as the ICCD recording over a single frame (b) and multiple frames (c,d). We note that the microdischarge lifetime (in the order of 10 ns) is much smaller than the time window of a single frame (0.1 ms).

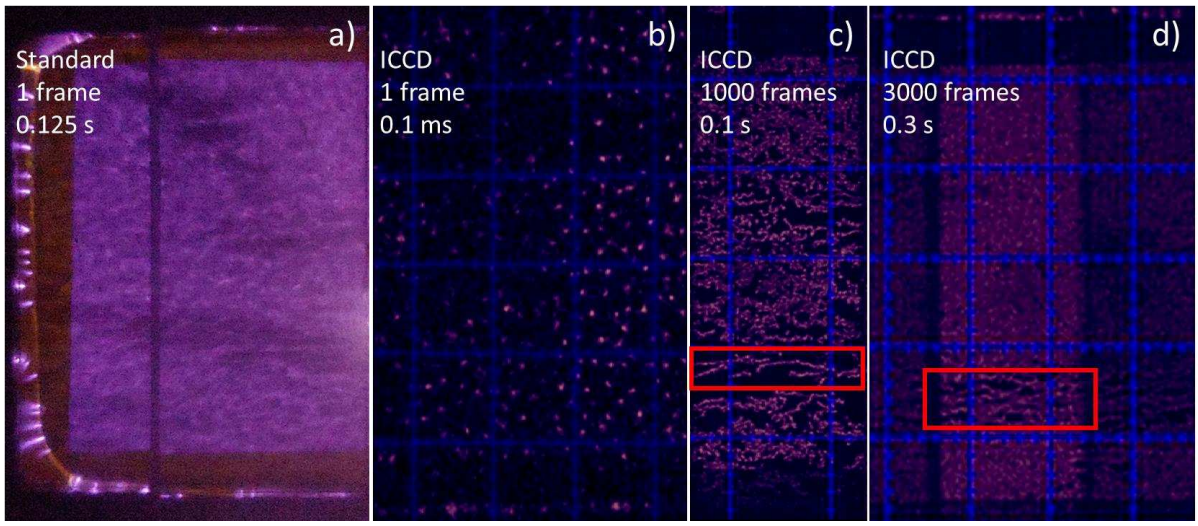

Figure 13. Photograph of a filamentary DBD plasma, driven at 12 kHz and 100 W (a), and ICCD recording of a single frame (0.1 ms, b) and multiple frames (i.e., 1,000 frames, 0.1 s (c) and 3,000 frames, 0.3 s (d)). The size of the grid is 10 x 10 mm^2.

From figure 13 we can conclude that a uniform distribution of microdischarges is indeed an adequate assumption when considering typical time scales associated with the residence time (i.e., seconds). We note however that the exact behaviour may depend on the discharge frequency, which will affect the randomness of the microdischarges due to the memory effect, leading to the self-organization of microdischarges as reported in literature [29], [30]. Those effects were also observed in our own experiments (not shown), but we note that such self-organized microdischarge distributions typically still cover the whole reactor volume, which means that this effect does not significantly impact the assumption behind our Monte Carlo calculations. Also the gas flow can influence the microdischarge location [30]. This can also be seen in figures 13c and 13d, where microdischarges follow a path in the direction of the gas flow (from left to right) creating aligned dots instead of random dots (indicated in the red boxes). This effect was observed to be more pronounced at higher discharge frequencies, which is also attributed to the memory effect. The microdischarges moving with the gas flow, might be an effect that increases the total duration during which a gas molecule is exposed to the strong microdischarges. In general, we judge that our assumptions on the uniform distribution of microdischarges, as used in the Monte Carlo calculations, is valid from 4 to 30 kHz, based on our experimental observations.

Finally, the operating pressure could influence the above observations and thus the assumptions behind the Monte Carlo calculations should be re-evaluated for such cases, i.e., low pressure conditions. However, low pressure plasmas are typically more homogeneous and thus do not exhibit the filamentary microdischarges of interest [31]. The memory effect is typically also a function of pressure due to the change in mean free path of the gas particles [32].

3.4. Experimental and calculated plasma-catalytic NH_3 yield

We now want to verify whether the concept of the fraction of microdischarges, as calculated in section 3.2, really has a physical meaning and whether our proposed relationship (i.e., the fraction of microdischarges is the ratio of microdischarge volume over the reactor gas volume) provides a realistic value. Therefore, we applied this concept to plasma-catalytic NH_3 synthesis, using our previously developed plasma chemistry and catalytic surface chemistry microkinetics models [21], by running them as a function of residence time, and comparing with plasma-catalytic NH_3 synthesis experiments in a packed bed DBD with Co catalyst on Al_2O_3 beads, at different residence times.

We now adopt the exact microdischarge volume of 0.088 mm^3 of our previous study, which is also related to the plasma power density in the model [21]. The relevant reactor volume after packing was 6.4 cm^3, which gives a fraction of microdischarges of 1.37×10^{-5}. Again assuming 25 microdischarges per discharge half cycle and a discharge frequency of 23.5 kHz, following our experimental conditions, gives a microdischarge frequency of 1,175,000 s^{-1} (i.e., $2N_{MD,½\ cycle}f_D$, cf. also equation 4) and 16 s^{-1} after applying the above fraction of microdischarges (i.e., $\eta_{MD}2N_{MD,½\ cycle}f_D$, cf. also equation 5). The

simulation provides the NH_3 concentration as a function of time, for a total residence time of 3.84 s [21], which corresponds to 61 microdischarges that will be considered in the model, based on the above fraction of microdischarges. The experiments were performed for different flow rates, ranging between 100 and 400 ml/min, thus yielding different residence times ranging from 1.0 to 3.8 s, which can directly be compared to the time dependence in the model.

In figure 14, we compare the experimental results against the calculated results, obtained by performing a sensitivity analysis by varying the fraction of microdischarges over four orders of magnitude (between 10^{-6} and 10^{-2}, figure 14a) and within the same order of magnitude (between 0.5×10^{-5} and 9.0×10^{-5}, figure 14b).

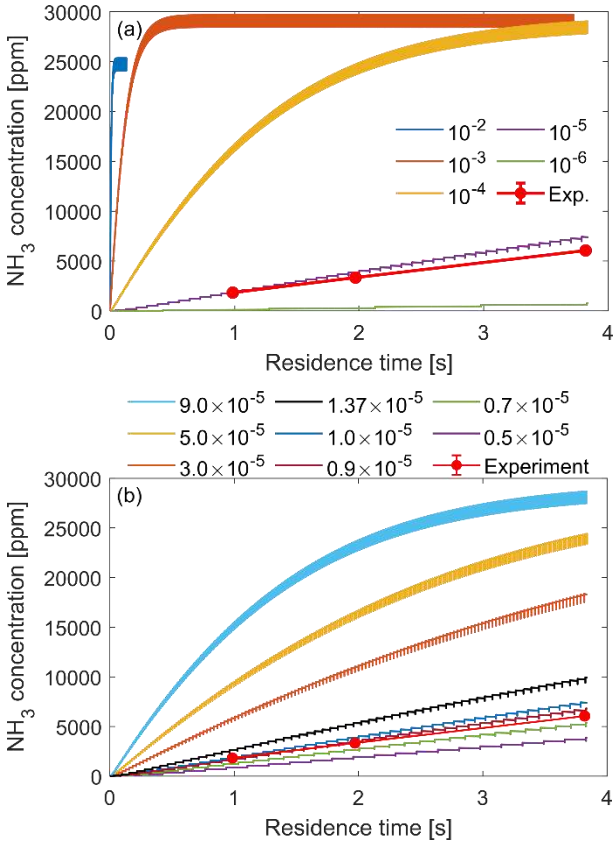

Figure 14. Calculated NH_3 concentration as a function of residence time, for different fractions of microdischarges, compared to experimentally obtained values (Exp.). The fraction of microdischarges is varied over four orders of magnitude in (a) and within the same order of magnitude in (b).

It is clear that a much larger or smaller fraction of microdischarges gives unrealistically fast and slow NH_3 synthesis rates (cf. figure 14a). This confirms that the order of magnitude of the fraction of microdischarges, as obtained by our combined particle tracing and Monte Carlo simulations, appears realistic. Figure 14b shows that the results are quite sensitive to the assumption of the fraction of microdischarges, i.e., even a factor 2 makes a large difference. The experimental data agrees best with a fraction of microdischarges of 0.9×10^{-5}, which is slightly lower than the value of 1.37×10^{-5}, based on the assumed microdischarge volumes [21]. However, we note that the chosen discharge volumes, the

resulting power density and thus the plasma kinetics are subject to uncertainties. Nevertheless, the agreement is still very reasonable; the fraction of microdischarges yielding best agreement with the experiments is close to the value predicted by the empirical relationship (microdischarge volume over reactor gas volume) as discussed in section 3.2, and the value resulting from the combined particle tracing and Monte Carlo modelling approach. This indicates that our combined particle tracing and Monte Carlo simulations method can provide a realistic picture of the fraction of microdischarges experienced by the gas molecules.

In figure 15 we plot the NH_3 concentration at the end of the reactor as a function of the fraction of microdischarges, with the latter both on a linear scale and logarithmic scale (inset, to cover a larger range). We can see that the NH_3 concentration increases with the fraction of microdischarges, but for a larger fraction of microdischarges (between 10^{-4} and 10^{-3}), it remains fairly constant, and for still larger fractions, it starts to drop (see inset in the figure). This is attributed to the interpulse time. When molecules experience more microdischarges (corresponding to a large fraction of microdischarges), the interpulse time is smaller (e.g., in the order of 100 ms and 100 µs for a fraction of microdischarges of 10^{-5} and 10^{-2}, respectively). In our previous study, we found that NH_3 is net produced in between the microdischarges and net destroyed during the microdischarges themselves. However, one so-called microdischarge and afterglow pair causes a net NH_3 gain, until a steady state is reached [21]. Based on these considerations, we indeed expect that there is an optimal interpulse time, which we find between 1 and 10 ms (i.e., a microdischarge fraction between approximately 10^{-3} and 10^{-4}, respectively) based on figure 15.

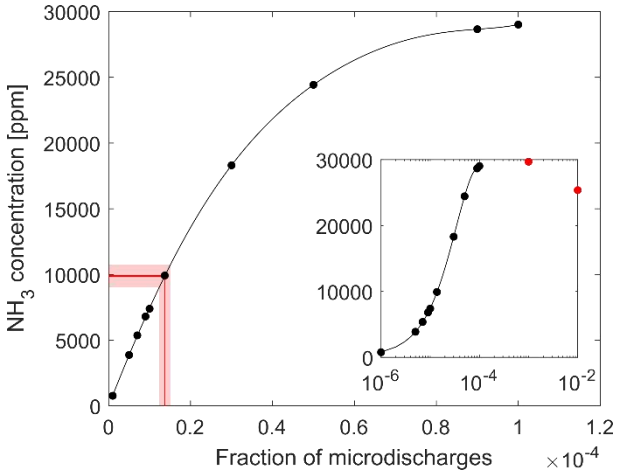

Figure 15. Calculated NH_3 concentration at the end of the reactor as a function of the fraction of microdischarges on both a linear scale and logarithmic scale (inset, with 2 extra data points (red dots)). A microdischarge fraction of 1.37×10^{-5} is indicated with a 1 % and 10 % spread (dark and light red areas, respectively).

The Monte Carlo calculations resulted in fractions of microdischarges with typical uncertainties, less than 1 %. However, we note that this is the average behaviour and that the gas could also be described with a microdischarge fraction distribution, by evaluating the fraction of microdischarges for each

particle trajectory individually. Assuming the average fraction of microdischarges of 1.37×10^{-5} and an uncertainty of 1 % gives an NH_3 concentration of 9880 ± 90 ppm (cf. figure 15). A difference of 3, 5 or 10 %, which could be relevant when considering an actual microdischarge fraction distribution, would give a difference of 260, 430 and 870 ppm, respectively.

3.5. Generalization of the concept: fraction of plasma power transferred to the gas molecules

The fraction of microdischarges experienced by the molecules can be considered as a plasma characteristic of a filamentary DBD. At the same time, however, this quantity directly represents the fact that not all power put into the plasma is equally transferred to each molecule [15]. In other words, gas molecules only see a fraction of the power put into the plasma. This is a direct consequence of the non-uniformity and stochastic behaviour of the plasma. Gas molecules would only be able to experience all the plasma power if a plasma is perfectly uniform (i.e., constant plasma power density) in space and time, and if it occupies the entire reactor, such that all gas molecules passing through the reactor would effectively pass through the plasma region and experience the same plasma power. Either plasma non-uniformity or stochastic behaviour of e.g., microdischarges will reduce the fraction of power transferred to the individual molecules, as these effects give rise to individual gas molecules being treated differently by the plasma.

As discussed above, the fraction of microdischarges can be generalized to the fraction of power transferred to each molecule, and this quantity can in principle be defined for any plasma and is related to both spatial and temporal plasma (non)uniformity. It can be considered as a kind of "plasma reactor efficiency". For instance, in a gliding arc (GA) plasma, only a limited fraction of the gas molecules actually passes through the active arc plasma, as the latter does not occupy the entire reactor volume, and this limits the "plasma reactor efficiency" [33]–[35]. The same was observed in an atmospheric pressure glow discharge (APGD) [36]. For a DBD, this fraction of power transferred would correspond to the fraction of microdischarges experienced by the molecules, giving rise to a very low "plasma reactor efficiency" (i.e., order of 0.001 %). However, this reasoning assumes that the entire applied plasma power is deposited in the microdischarges. In our recent study on plasma-catalytic NH_3 synthesis, we considered typical current-voltage characteristics of our packed bed DBD and found that a significant portion of the applied power still gives rise to a uniform plasma power (related to surface discharges at the packing beads [24]). In other words, only part of the input power is transferred to the microdischarges. In that case, the "plasma reactor efficiency" can be even close to 50 % [21]. This could explain the higher efficiency of a packed bed DBD (characterized by a combination of filamentary and surface microdischarges) compared to an empty DBD (characterized by only filamentary microdischarges), as often reported in plasma-catalytic experiments [37]–[41].

Finally, we note that a filamentary plasma, which, according to the above discussion, would have a lower "plasma reactor efficiency", typically exhibits much stronger plasma conditions compared to

uniform plasmas, which would correspond to higher "plasma reactor efficiencies". This means that both types of plasmas are of interest in their own way, and warrant further investigation, due to completely different underlying mechanisms and chemical kinetics.

4. Conclusions

We performed particle tracing simulations through both an empty and packed bed DBD reactor, typically used for plasma catalysis. In the packed bed reactor, we placed approximately 13,000 hard sphere beads in the gap between two concentric cylinders. We discussed in detail the flow characteristics and residence time distribution of the gas molecules in both an empty and packed bed DBD. We showed that the addition of a packed bed creates viscous boundary layers that slow down the gas in the centre of the packed bed where two packing bead layers are near to each other. Furthermore we showed that nearly 90% of the gas is redistributed towards the wall of the reactor, where there is a relatively large distance between the reactor wall and the packing beads.

The calculated particle trajectories were used in a Monte Carlo calculation, mimicking a filamentary DBD, to determine the fraction of microdischarges experienced by a single gas molecule. The results provided evidence for an empirical expression of this fraction of microdischarges, that is, the fraction of microdischarges is roughly equal to the microdischarge volume over the reactor gas volume.

To verify whether this proposed relationship (i.e., the fraction of microdischarges is the ratio of microdischarge volume over the reactor gas volume) provides a realistic value, we performed plasma and catalyst surface kinetics simulations for plasma-catalytic NH_3 synthesis, in which the fraction of microdischarges was used as input, and we compared the calculated NH_3 concentration as a function of time with experimental data. The experimental results could only be reproduced when the fraction of microdischarges was consistent with the definition based of microdischarge volume over reactor gas volume. The modelling results were highly sensitive to the assumed fraction of microdischarges, but a good agreement was obtained with the predicted value from the Monte Carlo simulations, which validates our concept of the fraction of microdischarges.

Finally, we can generalize the fraction of microdischarges, as it actually represents the fraction of plasma power transferred to the gas molecules. Indeed, not all power will be transferred to each molecule when the plasma is spatially and temporally non-uniform, and this principle is valid for other plasma types than DBDs as well, such as GA plasma or APGD. Based on these principles, we can define a "plasma reactor efficiency", which in case of a DBD plasma can be directly related to the fraction of microdischarges.

Acknowledgements

This research was supported by the Excellence of Science FWO-FNRS project (FWO grant ID GoF9618n, EOS ID 30505023), the European Research Council (ERC) under the European Union's

Horizon 2020 research and innovation programme (grant agreement No 810182 – SCOPE ERC Synergy project) and by the Flemish Government through the Moonshot cSBO project P2C (HBC.2019.0108). The calculations were performed using the Turing HPC infrastructure at the CalcUA core facility of the Universiteit Antwerpen (UAntwerpen), a division of the Flemish Supercomputer Center VSC, funded by the Hercules Foundation, the Flemish Government (department EWI) and the UAntwerpen. The authors would also like to thank Hamid Ahmadi Eshtehardi for discussions on the plasma-kinetic DBD model and Yannick Engelmann for discussions on the surface kinetics model.

References

[1] A. Bogaerts, X. Tu, J. C. Whitehead, G. Centi, L. Lefferts, O. Guaitella, F. Azzolina-Jury, H.-H. Kim, A. B. Murphy, W. F. Schneider, T. Nozaki, J. C. Hicks, A. Rousseau, F. Thevenet, A. Khacef, M. Carreon, "The 2020 plasma catalysis roadmap," *J. Phys. D. Appl. Phys.*, vol. 53, p. 443001, 2020.

[2] K. H. R. Rouwenhorst, Y. Engelmann, K. van 't Veer, R. S. Postma, A. Bogaerts, and L. Lefferts, "Plasma-driven catalysis: green ammonia synthesis with intermittent electricity," *Green Chem.*, vol. 22, pp. 6258–6287, 2020.

[3] A. Ozkan, T. Dufour, A. Bogaerts, and F. Reniers, "How do the barrier thickness and dielectric material influence the filamentary mode and CO2 conversion in a flowing DBD?," *Plasma Sources Sci. Technol.*, p. 45016, 2016.

[4] W. Wang, R. Snoeckx, X. Zhang, M. S. Cha, and A. Bogaerts, "Modeling Plasma-based CO2 and CH4 Conversion in Mixtures with N2, O2, and H2O: The Bigger Plasma Chemistry Picture," *J. Phys. Chem. C*, vol. 122, no. 16, pp. 8704–8723, 2018.

[5] M. M. Turner, "Uncertainty and error in complex plasma chemistry models," *Plasma Sources Sci. Technol.*, vol. 24, p. 035027, 2015.

[6] M. M. Turner, "Uncertainty and sensitivity analysis in complex plasma chemistry models," *Plasma Sources Sci. Technol.*, vol. 25, p. 015003, 2016.

[7] L. L. Alves, A. Bogaerts, V. Guerra, and M. M. Turner, "Foundations of modelling of nonequilibrium low-temperature plasmas," *Plasma Sources Sci. Technol.*, vol. 27, p. 023002, 2018.

[8] R. Aerts, T. Martens, and A. Bogaerts, "Influence of Vibrational States on CO2 Splitting by Dielectric Barrier Discharges," *J. Phys. Chem. C*, vol. 116, pp. 23257–23273, 2012.

[9] R. Snoeckx, R. Aerts, X. Tu, and A. Bogaerts, "Plasma-Based Dry Reforming: A Computational Study Ranging from the Nanoseconds to Seconds Time Scale," *J. Phys. Chem. C*, vol. 4, 2013.

[10] R. Snoeckx, M. Setareh, R. Aerts, P. Simon, A. Maghari, and A. Bogaerts, "Influence of N2 concentration in a CH4/N2 dielectric barrier discharge used for CH4 conversion into H2," *Int. J. Hydrogen Energy*, vol. 38, no. 36, pp. 16098–16120, 2013.

[11] T. Kozak and A. Bogaerts, "Splitting of CO2 by vibrational excitation in non-equilibrium plasmas: a reaction kinetics model," *Plasma Sources Sci. Technol.*, vol. 23, 2014.

[12] R. Aerts, W. Somers, and A. Bogaerts, "Carbon Dioxide Splitting in a Dielectric Barrier Discharge Plasma: A Combined Experimental and Computational Study," *ChemSusChem*, vol. 8, pp. 702–716, 2015.

[13] R. Snoeckx, A. Ozkan, F. Reniers, and A. Bogaerts, "The Quest for Value-Added Products from Carbon Dioxide and Water in a Dielectric Barrier Discharge: A Chemical Kinetics Study,"

ChemSusChem, vol. 10, pp. 409–424, 2017.

[14] A. Bogaerts, W. Wang, A. Berthelot, and V. Guerra, "Modeling plasma-based CO2 conversion: crucial role of the dissociation cross section," *Plasma Sources Sci. Technol.*, vol. 25, 2016.

[15] K. van 't Veer, F. Reniers, and A. Bogaerts, "Zero-dimensional modelling of unpacked and packed bed dielectric barrier discharges: The role of vibrational kinetics in ammonia synthesis," *Plasma Sources Sci. Technol.*, vol. 29, no. 4, p. 045020, 2020.

[16] B. E. Poling, J. M. Prausnitz, and J. P. O'Connell, *The properties of Gases and Liquids*, 5th ed. 2000.

[17] F. R. Menter, "Zonal Two-Equation k-ω Turbulence Model for Aerodynamic Flows," in *AIAA Paper*, 1993, pp. 1993–2906.

[18] COMSOL Multiphysics® v. 5.5. www.comsol.com. COMSOL AB, Stockholm, Sweden.

[19] M. Gao, Y. Zhang, H. Wang, B. Guo, Q. Zhang, and A. Bogaerts, "Mode Transition of Filaments in Packed-Bed Dielectric Barrier Discharges," *catalysts*, vol. 8, p. 248, 2018.

[20] Y. Engelmann, K. van 't Veer, Y. Gorbanev, E. Vlasov, Y. Yi, E. C. Neyts, S. Bals, W. F. Schneider, A. Bogaerts, "Plasma catalysis for ammonia synthesis: the importance of Eley-Rideal reactions," *submitted*

[21] K. van 't Veer, Y. Engelmann, F. Reniers, and A. Bogaerts, "Plasma-Catalytic Ammonia Synthesis in a DBD Plasma: Role of Microdischarges and Their Afterglows," *J. Phys. Chem. C*, vol. 124, pp. 22871–22883, 2020.

[22] S. Pancheshnyi, B. Eismann, G. J. M. Hagelaar, and L. C. Pitchford, "Computer code ZDPlasKin."

[23] G. J. M. Hagelaar and L. C. Pitchford, "Solving the Boltzmann equation to obtain electron transport coefficients and rate coefficients for fluid models," *Plasma Sources Sci. Technol.*, vol. 14, 2005.

[24] W. Wang, H. Kim, K. Van Laer, and A. Bogaerts, "Streamer propagation in a packed bed plasma reactor for plasma catalysis applications," *Chem. Eng. J.*, vol. 334, no. September 2017, pp. 2467–2479, 2018.

[25] J. Kruszelnicki, K. W. Engeling, and J. E. Foster, "Propagation of negative electrical discharges through 2-dimensional packed bed reactors," *J. Phys. D. Appl. Phys.*, vol. 50, p. 25203, 2017.

[26] K. W. Engeling, J. Kruszelnicki, and M. J. Kushner, "Time-resolved evolution of micro-discharges, surface ionization waves and plasma propagation in a two-dimensional packed bed reactor," *Plasma Sources Sci. Technol.*, vol. 27, p. 085002, 2018.

[27] Z. Mujahid, J. Kruszelnicki, A. Hala, and M. J. Kushner, "Formation of surface ionization waves in a plasma enhanced packed bed reactor for catalysis applications," *Chem. Eng. J.*, vol. 382, 2020.

[28] Y. Wang *et al.*, "Plasma-Enhanced Catalytic Synthesis of Ammonia over a Ni/Al2O3 Catalyst at Near-Room Temperature: Insights into the Importance of the Catalyst Surface on the Reaction Mechanism," *ACS Catal.*, vol. 9, pp. 10780–10793, 2019.

[29] H. Itoh, K. Kobayashi, K. Teranishi, N. Shimomura, and S. Suzuki, "Time-Resolved Observation of Self-Organized Filaments Formed in a Helium-Dielectric Barrier Discharge," *IEEE Trans. Plasma Sci.*, vol. 39, no. 11, pp. 2204–2205, 2011.

[30] Y. Yang, Y. I. Cho, G. Friedman, A. Fridman, and G. Fridman, "Self-Organization and Migration of Dielectric Barrier Discharge Filaments in Argon Gas Flow," *IEEE Trans. Plasma Sci.*, vol. 39, no. 11, pp. 2060–2061, 2011.

[31] B. Eliasson and U. Kogelschatz, “Modeling and Applications of Silent Discharge Plasmas,” *IEEE Trans. Plasma Sci.*, vol. 19, pp. 309–323, 1991.

[32] F. Massines, N. Gherardi, and N. Naud, “Recent advances in the understanding of homogeneous dielectric barrier discharges,” *Eur. Phys. J. Appl. Phys.*, vol. 47, p. 22805, 2009.

[33] M. Ramakers, G. Trenchev, S. Heijkers, W. Wang, and A. Bogaerts, “Gliding Arc Plasmatron: Providing an Alternative Method for Carbon Dioxide Conversion,” *ChemSusChem*, vol. 10, pp. 2642–2652, 2017.

[34] S. Heijkers and A. Bogaerts, “CO2 Conversion in a Gliding Arc Plasmatron: Elucidating the Chemistry through Kinetic Modeling,” *J. Phys. Chem. C*, vol. 121, pp. 22644–22655, 2017.

[35] S. R. Sun, H. X. Wang, D. H. Mei, X. Tu, and A. Bogaerts, “CO2 conversion in a gliding arc plasma: Performance improvement based on chemical reaction modeling,” *J. CO2 Util.*, vol. 17, pp. 220–234, 2017.

[36] G. Trenchev, A. Nikiforov, W. Wang, S. Kolev, and A. Bogaerts, “Atmospheric pressure glow discharge for CO2 conversion: Model-based exploration of the optimum reactor configuration,” *Chem. Eng. J.*, vol. 362, no. December 2018, pp. 830–841, 2019.

[37] X. Duan, Z. Hu, Y. Li, and B. Wang, “Effect of Dielectric Packing Materials on the Decomposition of Carbon Dioxide Using DBD Microplasma Reactor,” *AIChE J.*, vol. 61, no. 3, 2015.

[38] K. Van Laer and A. Bogaerts, “Improving the Conversion and Energy Efficiency of Carbon Dioxide Splitting in a Zirconia-Packed Dielectric Barrier Discharge Reactor,” *Energy Technol.*, vol. 3, pp. 1038–1044, 2015.

[39] Y. Zeng, X. Zhu, D. Mei, B. Ashford, and X. Tu, “Plasma-catalytic dry reforming of methane over y-Al2O3 supported metal catalysts,” *Catal. Today*, vol. 256, pp. 80–87, 2015.

[40] I. Michielsen, Y. Uytdenhouwen, J. Pype, B. Michielsen, J. Mertens, F. Reniers, V. Meynen, A. Bogaerts, “CO2 dissociation in a packed bed DBD reactor: First steps towards a better understanding of plasma catalysis,” *Chem. Eng. J.*, vol. 326, pp. 477–488, 2017.

[41] Y. Uytdenhouwen, V. Meynen, P. Cool, and A. Bogaerts, “The Potential Use of Core-Shell Structured Spheres in a Packed-Bed DBD Plasma Reactor for CO2 Conversion,” *catalysts*, vol. 10, p. 530, 2020.